Intrinsic AMOC Eigenmodes for Bond-Cycle Variability

Xiangying Zhou[a,b], Haijun Yang*[a], and Shuxiang Wang[a]

[a] *Department of Atmospheric and Oceanic Sciences and Key Laboratory of Polar Atmosphere-ocean-ice System for Weather and Climate of Ministry of Education, Fudan University, Shanghai, 200438, China*

[b] *MARUM–Center for Marine Environmental Sciences, University of Bremen, Bremen, 28359, Germany*

Climate Dynamics
1st submission,
July 18, 2026

Corresponding author: Haijun Yang, yanghj@fudan.edu.cn

Key contributions:

1. Identification of two intrinsic AMOC eigenmodes.
2. Demonstration that background climate modifies their period and damping rather than creating new oscillations.
3. Recognition that damping controls whether an intrinsic mode is expressed in paleoclimate records.

ABSTRACT

Millennial-scale climate variability is a prominent feature of Holocene climate records and is commonly represented by the Bond cycle. Although numerous proxy records document Bond-like variability, its physical origin remains poorly understood. Here, we investigate the dynamical origin of millennial-scale variability using a conceptual model of the Atlantic Meridional Overturning Circulation (AMOC). Linear stability analysis identifies two intrinsic oscillatory AMOC eigenmodes: a weakly unstable multicentennial mode and a strongly damped millennial mode. We show that the multicentennial mode shifts into the millennial range under a weakened mean AMOC, whereas the intrinsic millennial mode becomes weakly damped through feedback from Antarctic Bottom Water (AABW). Under a sufficiently freshened Southern Ocean background, stochastic forcing can efficiently excite the weakly damped millennial mode, leading to sustained oscillations with periods comparable to those inferred for the Bond cycle. These results suggest that Bond-cycle variability may reflect the climatic expression of intrinsic AMOC eigenmodes, whose characteristic timescales and damping properties are strongly modulated by the background state of the overturning circulation. More broadly, our results suggest that the observability of intrinsic climate modes depends not only on their characteristic periods, but also on their damping rates, providing a possible explanation for the apparent discrepancy between paleoclimate records and coupled climate model simulations.

KEYWORDS: Atlantic Meridional Overturning Circulation (AMOC), Antarctic Bottom Water (AABW), Bond cycle, Millennial climate variability, Linear stability analysis

Significance: This study provides a dynamical framework for understanding Bond-cycle variability from the perspective of intrinsic AMOC eigenmodes. Rather than invoking a distinct millennial oscillation mechanism, we show that Bond-cycle variability may arise from intrinsic AMOC modes whose periods and damping rates are regulated by the background overturning circulation. By identifying two eigenmodes and separating the controls on period and damping, our results provide a coherent explanation for why millennial variability appears intermittently in paleoclimate records but is often not captured in coupled climate model simulations.

1. Introduction

Proxy data and climate reconstructions indicate that the climate system has experienced millennial-scale variability during different geological periods. Such variability is prominently manifested in the abrupt Dansgaard–Oeschger (D-O) events during glacial periods (Dansgaard et al. 1984) and in Bond-event-like variability during the Holocene (Bond et al. 1997; von der Heydt et al. 2021). Although the boundary conditions of glacial periods and the Holocene differed substantially, Bond et al. (1997) suggested that Bond events and D-O events exhibit a statistically similar pacing, together forming a sequence of millennial-scale climate events with a characteristic period of about 1470 ± 500 years. Because both types of events involve planetary-scale redistribution of heat and salt between hemispheres, as well as the interactions between surface forcing and deep-ocean adjustment, the Atlantic Meridional Overturning Circulation (AMOC) has long been considered as a fundamental component of their dynamics and a potential source of millennial-scale climate variability (Sakai and Peltier 1995; Sakai and Peltier 1996).

Despite their broadly similar timescales, D-O events and Bond events occurred under markedly different climatic background states and likely involved different amplitudes and mechanisms. D-O events developed under glacial conditions and were characterized by large-amplitude, abrupt climate changes. During D-O cold phases, the AMOC was likely weak or even collapsed, whereas during warm phases it was substantially stronger (Lynch-Stieglitz 2017). D-O-like variability has been reproduced in a wide range of climate models (Arzel et al. 2010; Colin de Verdière 2007; Friedrich et al. 2010; Sévellec and Fedorov 2014; Winton and Sarachik 1993). Correspondingly, a relatively mature theoretical understanding of D-O events has emerged, including mechanisms involving AMOC multiple equilibria (Ganopolski and Rahmstorf 2001, 2002; Timmermann et al. 2003), internal ocean dynamics including deep-decoupling oscillations (Colin de Verdière 2007; Gottwald 2021; Olsen et al. 2005; Winton and Sarachik 1993), and ice-sheets and sea-ice feedbacks (Colin De Verdière and Te Raa 2010; Peltier and Vettoretti 2014; Vettoretti and Peltier 2018; Vettoretti et al. 2022; Wang and Mysak 2006; Zhang et al. 2014).

Compared with D-O events, the dynamical origin of Bond-event variability remains much less understood. In particular, a fundamental question remains largely unexplored: does the AMOC itself possess an intrinsic millennial-scale oscillatory mode under Holocene conditions? In this study, we focus on Bond-event-like millennial variability under Holocene-like background conditions. Bond events occurred during the relatively warm and stable Holocene and exhibited substantially smaller amplitudes than D-O events. These events may also be linked to internal variability of the climate system (Debret et al. 2007; Khider et al. 2014; Schulz et al. 2007). An implicit assumption underlying most previous studies is that Bond-cycle variability requires a distinct millennial oscillation mechanism. However, this assumption has rarely been examined. If the AMOC already possesses an intrinsic oscillatory mode, Bond-cycle variability may instead reflect changes in the period and damping of that mode under different climate backgrounds, rather than the emergence of a fundamentally new oscillation.

In comprehensive coupled climate models, millennial-scale AMOC variability may involve freshwater forcing, sea-ice feedbacks, Southern Ocean processes, stochastic atmospheric forcing, and coupled ocean–atmosphere interactions (e.g., Ganopolski and Rahmstorf 2002; Klockmann et al. 2020; Peltier and Vettoretti 2014; Vettoretti and Peltier 2018; Vettoretti et al. 2022; Zhang et al. 2017). Because these processes are strongly coupled and operate simultaneously, it is often difficult to isolate the fundamental dynamical mechanism responsible for millennial-scale variability. Conceptual models provide a complementary approach by isolating the minimum dynamical ingredients required to generate low-frequency oscillations. Earlier box-model studies demonstrated that thermohaline circulation can exhibit damped, unstable, or self-sustained oscillations through salinity-advection feedbacks and the finite adjustment time of the overturning circulation (Griffies and Tziperman 1995; Huang et al. 1992; Stommel 1961). However, these studies have focused primarily on multicentennial variability, leaving the existence and physical origin of an intrinsic millennial-scale AMOC eigenmode largely unexplored.

Our previous study identified a weakly unstable multicentennial eigenmode of the AMOC (Zhou et al. 2026). That mode is primarily controlled by North Atlantic salinity-advection feedback and can become self-sustained when weak nonlinear mixing is included in the subpolar North Atlantic. The same linear system also contains a second oscillatory eigenmode with a millennial-scale period. Unlike the multicentennial mode, however, this millennial eigenmode is strongly damped under present-day climate conditions and was therefore only briefly noted in the previous study. The coexistence of these two eigenmodes suggests that the thermohaline circulation possesses multiple intrinsic low-frequency timescales, with the millennial branch warranting further investigation.

In this study, we investigate the physical origin and climatic relevance of the intrinsic millennial AMOC eigenmodes. We first demonstrate that the weakly unstable multicentennial eigenmode can shift into the millennial range under a substantially weakened mean AMOC. We then show that feedback from the Antarctic Bottom Water (AABW) cell reduces the damping of the intrinsic millennial eigenmode. Under a sufficiently freshened Southern Ocean background, this weakly damped mode can be efficiently excited by stochastic forcing, producing sustained millennial-scale variability comparable to the Bond cycle. Overall, our results suggest that Bond-cycle variability may be explained by intrinsic AMOC eigenmodes, whose periods and damping characteristics are strongly controlled by the background state of the overturning circulation.

The remainder of the paper is organized as follows. Section 2 describes the idealized two-hemisphere salinity-only model. Section 3 investigates the transition of the weakly unstable multicentennial eigenmode to millennial timescales under a weakened AMOC. Section 4 examines the intrinsic millennial eigenmode and its excitation through AABW feedback and stochastic forcing. Finally, Section 5 provides the conclusions and discussions.

2. Two-hemisphere box model

a. Model description

We use the two-hemisphere six-box model developed by Zhou et al. (2026), which divides the Atlantic basin into three meridional regions: the subpolar North Atlantic, the tropical Atlantic, and the subpolar South Atlantic, each consisting of an upper and a lower box (Fig. 1). Boxes 1–3 denote the upper ocean from north to south, and boxes 4–6 denote the corresponding lower-ocean boxes.

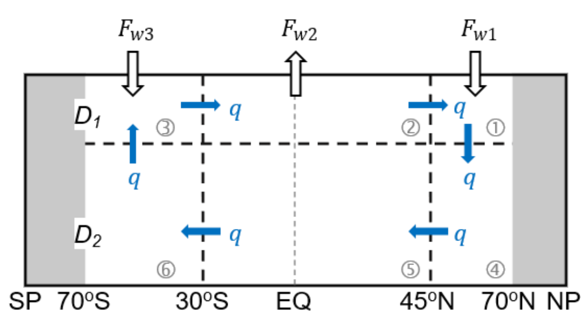

FIG. 1. Schematic diagrams of two-hemispheric ocean six-box models. The circled numbers (e.g., ① and ②) denote the ocean boxes. Boxes 1 and 4 represent the upper and lower subpolar North Atlantic, respectively; boxes 2 and 5 represent the upper and lower tropical oceans, respectively; boxes 3 and 6 represent the upper and lower subpolar South Atlantic, respectively. D_1 and D_2 are the depths of the upper and lower oceans,

respectively. F_{w1}, F_{w2}, and F_{w3} are the virtual salt fluxes into boxes 1-3, representing surface freshwater fluxes in reality. q represents the AMOC.

The full six-box model and its governing equations are described in detail in Zhou et al. (2026). Here, we use the linearized salinity equations,

$$V_1\dot{S}_1' = \bar{q}(S_2' - S_1') + q'(\bar{S}_2 - \bar{S}_1), \tag{1a}$$

$$V_2\dot{S}_2' = \bar{q}(S_3' - S_2') + q'(\bar{S}_3 - \bar{S}_2), \tag{1b}$$

$$V_3\dot{S}_3' = \bar{q}(S_6' - S_3') + q'(\bar{S}_6 - \bar{S}_3), \tag{1c}$$

$$V_4\dot{S}_4' = \bar{q}(S_1' - S_4'), \tag{1d}$$

$$V_5\dot{S}_5' = \bar{q}(S_4' - S_5'), \tag{1e}$$

$$V_6\dot{S}_6' = \bar{q}(S_5' - S_6'). \tag{1f}$$

where V_i and S_i are the volume and salinity of box i, and $\bar{q}$ is the mean AMOC strength. The essential closure is that the AMOC anomaly (q') is linearly proportional to the density difference between the northern and southern subpolar boxes. In the salinity-only model, this reduces to a dependence on the subpolar salinity contrast:

$$q = \bar{q} + q' = \bar{q} + \lambda\Delta\rho' \tag{2}$$

$$\Delta\rho' = \rho_0\beta[\delta(S_1' - S_3') + (1-\delta)(S_4' - S_6')] \tag{3}$$

$$\delta = \frac{V_1}{V_1+V_4} = \frac{V_3}{V_3+V_6} = \frac{D_1}{D} \tag{4}$$

Here, λ is closure parameter, quantifying the sensitivity of the AMOC to salinity-induced changes in the meridional density gradient. The symbols ρ_0, β, D_1 and D denote the reference seawater density, the saline expansion coefficient, the upper-layer depth, and total ocean depth, respectively. The parameter values are listed in Table 1. This parameterization of the AMOC is adapted from the seminal work of Stommel (1961) and has since been widely adopted in numerous studies (e.g., Griffies and Tziperman 1995; Li and Yang 2022; Lucarini and Stone 2005a, 2005b; Rivin and Tziperman 1997; Scott et al. 1999; Yang et al. 2024).

A key extension of the present study is the explicit separation of the respective contributions of the North Atlantic Deep Water (NADW) and AABW cells to AMOC variability. In the previous study (Zhou et al. 2026), AMOC anomalies were assumed to arise solely from variability in the NADW cell. However, observational and modelling studies suggest that the NADW and AABW cells are dynamically coupled and often vary out of phase (e.g., Brix and Gerdes 2003; Frajka-Williams et al. 2011; Stössel and Kim 2001). To account for this interaction, the AMOC anomaly is decomposed into two components,

$$q' = q'_{NADW} + q'_{AABW} \tag{5}$$

where, q'_{NADW} and q'_{AABW} denote the contributions associated with variability in the NADW and AABW cells, respectively. The two components are parameterized separately in Sections 3 and 4 to examine their distinct roles in generating millennial-scale variability. The physical basis of this decomposition and the corresponding parameterizations is evaluated using a coupled climate model, as presented in Appendix B.

b. Parameter selection

The model parameters are chosen to represent present-day climatological conditions of the Atlantic overturning circulation. The basin volumes and equilibrium salinity distribution are chosen to be broadly consistent with CESM1 output (Yang et al. 2015), following Zhou et al. (2026). The reference AMOC strength is set to a realistic value consistent with observational estimates. These parameters define a base state about which linear stability analysis is performed. Sensitivity experiments are conducted by varying the mean AMOC strength (Section 3) and the upper Southern Ocean salinity (Section 4) to represent different climate backgrounds, including weakened overturning states and Southern Ocean freshening.

TABLE 1. Standard values of parameters and equilibria for the two-hemisphere model used in this study.

Symbol	Physical meaning	Value with units	Notes
L_1, L_2, L_3, L	Meridional scales of northern subpolar, tropical, southern subpolar ocean boxes, and the total scale	25°, 75°, 40°, 140°	Based on realistic geometry
D_1, D_2, D	Thicknesses of the upper, deeper, and their sum	1000, 3000, 4000 m	Based on realistic geometry
V_1	Volume of box 1	1.443×10^{16} m^3 (for 5200 km wide)	Based on realistic geometry
V_2, V_3, V_4, V_5, V_6	Volumes of boxes 2, 3, 4, 5, and 6	$3V_1$, $1.6V_1$, $3V_1$, $9V_1$, $4.8V_1$	Calculated from meridional scales and layer thicknesses
α	Thermal expansion coefficient	1.468×10^{-4} °C^{-1}	Commonly used values
β	Saline contraction coefficient	7.61×10^{-4} psu^{-1}	Commonly used values
ρ_0	Reference seawater density	1.0×10^{3} kg m^{-3}	Commonly used values
$\overline{S_1}$, $\overline{S_2}$, $\overline{S_3}$, $\overline{S_4}$, $\overline{S_5}$, $\overline{S_6}$	Equilibrium salinities of six boxes	33.9, 36.9, 33.8, 33.9, 33.9, 33.9 psu	Representative value from CESM1
$\bar{q}$	Equilibrium AMOC strength	20 Sv	Realistic value
λ	Linear closure coefficient of NADW cell	$17.8\ Sv\ kg^{-1}\ m^3$	Representative value from CESM
μ	Linear closure coefficient of AABW cell	$-10\ Sv\ kg^{-1}\ m^3$	Representative value from CESM

c. Linear stability analysis

The eigenvalues of the linearized six-box model are calculated numerically. Since the model contains six prognostic variables, the linear system possesses six eigenmodes. The real part of each eigenvalue determines the *e*-folding growth or decay rate of the corresponding mode, whereas the imaginary part determines its oscillation period.

For the reference parameter set (Table 1), the system exhibits four distinct types of eigenmodes (Table 2): (1) a weakly unstable oscillatory mode whose *e*-folding growth time (more than 1000 years) exceeds its oscillation period (about 400 years); (2) a strongly damped oscillatory mode whose *e*-folding decay time (around 50 years) is much shorter than its oscillation period (more than 2000 years); (3) a neutral mode corresponding to the equilibrium climate state; and (4) a purely damped non-oscillatory mode. In the following two sections, we investigate the two oscillatory eigenmodes separately and examine how they can give rise to millennial-scale variability under different background conditions. These two oscillatory eigenmodes form the basis of the subsequent analysis in Sections 3 and 4.

TABLE 2. Eigenvalues (ω) in two-hemisphere six-box model under the reference parameters in Table 1. Here, $\bar{q} = 20\ Sv$ and $\lambda = 17.8\ Sv\ kg^{-1}\ m^3$.

	Weakly unstable oscillatory mode	Strongly damped oscillatory mode	Zero mode	Purely damped mode
ω (unit in year)	$1066 \pm i409$	$-46 \pm i2145$	0	-19.8

3. Millennial oscillations from multicentennial eigenmode

The linear stability analysis of the six-box model reveals a weakly unstable multicentennial eigenmode for the reference parameter set. In this section, we investigate the first dynamical pathway by which this intrinsic mode can evolve into millennial-scale variability. Specifically, we examine how changes in the mean AMOC strength modify the characteristic timescale of this eigenmode. To isolate the mechanism controlling this eigenmode, we first consider a limiting case in which variability associated with the AABW cell is negligible, that is,

$$q' \approx q'_{NADW} \quad \text{and} \quad q'_{AABW} \approx 0. \tag{6}$$

Under this assumption, AMOC variability is controlled entirely by the NADW cell, and the overturning anomaly remains parameterized as a positive linear function of the meridional density difference between the two subpolar boxes [Eqs. (2)–(3)]. The closure parameter λ therefore quantifies the sensitivity of the NADW-driven AMOC anomaly to changes in the meridional density gradient.

a. Dependence of the eigenmode period on mean AMOC strength

The first question to address is what determines the characteristic period of the weakly unstable multicentennial eigenmode, and whether this intrinsic mode can evolve into a millennial-scale oscillation under a different mean climate state. Numerical linear stability analysis of the six-box model shows that the oscillation period increases systematically as the mean AMOC weakens.

For example, when $\bar{q} = 5\ Sv$, the oscillatory mode has a period of about 1600 years and an e-folding growth time of about 4900 years (Table 3; Fig. 2, green curve), indicating a weakly unstable millennial oscillation. When $\bar{q} = 10\ Sv$, the oscillatory period is approximately 800 years (Fig. 2, purple curve). This mode is still a quasi-millennial mode. When $\bar{q} = 20\ Sv$, the oscillatory period shifts to the multicentennial timescale (around 400 years) (Fig. 2, blue curve). In summary, as $\bar{q}$ increases, the imaginary part becomes larger, indicating a progressively shorter period (Table 3).

TABLE 3. Eigenvalues (ω) in two-hemisphere six-box model under different mean AMOC strengths.

	$\bar{q} = 5\ Sv$	$\bar{q} = 10\ Sv$	$\bar{q} = 20\ Sv$	Physical meaning
	$\lambda = 4.4\ Sv\ kg^{-1}m^3$	$\lambda = 8.9\ Sv\ kg^{-1}m^3$	$\lambda = 17.8\ Sv\ kg^{-1}m^3$	
ω (units in year)	$4937 \pm i1636$	$2132 \pm i818$	$1066 \pm i409$	Weakly unstable oscillatory mode

For a given mean AMOC strength, a larger λ implies a stronger AMOC response, thereby strengthening the salinity-advection feedback and making the oscillatory mode less stable. For example, when λ increases from 0 to 10 Sv $kg^{-1}\ m^3$ under $\bar{q} = 5\ Sv$, the AMOC becomes increasingly sensitive to changes in meridional density gradient, and the oscillatory mode gradually changes from damped to unstable (Fig. 2a, green curve). When $\lambda > 10$ Sv $kg^{-1}\ m^3$, the oscillatory eigenmodes disappear and are replaced by two purely growing modes. This indicates that when the salinity-advection feedback becomes excessively strong, the oscillatory adjustment is replaced by a monotonic instability.

Since λ affects the characteristics of the oscillatory eigenmodes, its value must be specified for the analysis. Unless otherwise stated, the closure parameter λ is chosen to maximize the imaginary part of the oscillatory eigenvalue (equivalently, to minimize the oscillation period) for each prescribed mean AMOC strength, as sensitivity tests show that the imaginary part of the eigenvalue varies only weakly near the selected value (Fig. 2, dashed vertical lines). This allows the dependence of the intrinsic timescale on $\bar{q}$ to be examined more clearly.

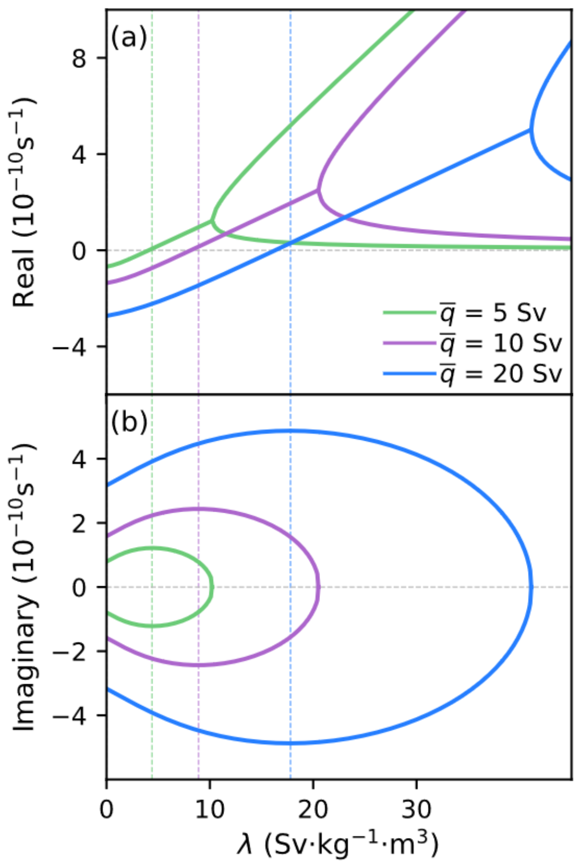

FIG. 2. Dependence of (a) the real parts and (b) the imaginary parts of the conjugate eigenvalues ω on λ (units: Sv kg^{-1} m^{3}) for the multicentennial oscillatory modes in the six-box model using the parameters in Table 1. The vertical dashed green, purple and blue lines correspond to λ = 4.4, 8.9, 17.8 Sv kg^{-1} m^{3} when Im(ω) of the oscillatory mode reaches the maximum. The units of the ordinate are 10^{-10} s^{-1}.

Although no closed-form analytical solution exists for the six-box model, the physical origin of this dependence can be understood from a simplified three-box model discussed in Zhou et al. (2026), in which the oscillation period satisfies

$$T \propto \frac{2\pi}{\bar{q}}\sqrt{(V_1+V_4)V_2} \tag{7}$$

where V_1, V_2, V_4 are the box volumes defined in Fig. 1. Eq. (7) is an analytical scaling relation, indicating that the characteristic period is inversely proportional to the mean AMOC strength ($\bar{q}$). Physically, a weaker overturning circulation requires a longer time to redistribute salinity anomalies between the two hemispheres, thereby lengthening the intrinsic oscillation period. Consequently, a sufficiently weak mean AMOC shifts the multicentennial eigenmode toward millennial timescales. The same dependence of the oscillation period on the mean overturning strength has also been identified in an independent two-dimensional idealized model (Wang et al. 2025, their Fig. 10), suggesting that this scaling is a robust property of thermohaline circulation rather than a specific feature of the simplified framework.

In summary, the linear stability analysis indicates that a sufficiently weak mean AMOC can shift the intrinsic multicentennial eigenmode into the millennial range. Under a climate background in which the AMOC is substantially weaker than at present, this dynamical pathway may provide favourable conditions for the emergence of Bond-event-like variability during warm climates, and potentially for D-O-like oscillations under glacial conditions.

b. Self-sustained millennial oscillations

The linear stability analysis presented above identifies a weakly unstable millennial eigenmode when the mean AMOC is sufficiently weak. However, linear theory only describes the initial growth of infinitesimal perturbations and cannot determine the finite-amplitude behavior of the system. To investigate whether this eigenmode can evolve into a sustained millennial oscillation, nonlinear processes that limit its growth must be included.

Several mechanisms have previously been proposed to produce finite-amplitude oscillations in thermohaline circulation models, including convection (Sévellec et al. 2006), nonlinear density-overturning relationships (Rivin and Tziperman 1997; Yang et al. 2024), and enhanced vertical mixing in the subpolar North Atlantic (Li and Yang 2022). Here we adopt the parameterization proposed by Li and Yang (2022), in which enhanced subpolar mixing counteracts the positive salinity-advection feedback and limits the oscillation amplitude. The formulations are summarized in Appendix A.

The nonlinear model is initialized by imposing a positive salinity anomaly ($S_1' = 0.5\ psu$) in the subpolar North Atlantic and integrated for more than 10,000 years. Figure 3 shows the resulting AMOC oscillations for different prescribed mean AMOC strengths. For all three mean AMOC states, the initially unstable eigenmode evolves into a finite-amplitude self-sustained oscillation (Fig. 3a). Consistent with the linear stability analysis, the oscillation period depends strongly on the mean AMOC strength, increasing from approximately 400 years for $\bar{q} = 20\ Sv$ to about 800 years for $\bar{q} = 10\ Sv$ and 1600 years for $\bar{q} = 5\ Sv$ (Fig. 3b). The close agreement between the nonlinear integrations and the eigenvalue analysis indicates that nonlinear mixing primarily limits the oscillation amplitude, whereas the intrinsic period is determined by the underlying eigenmode.

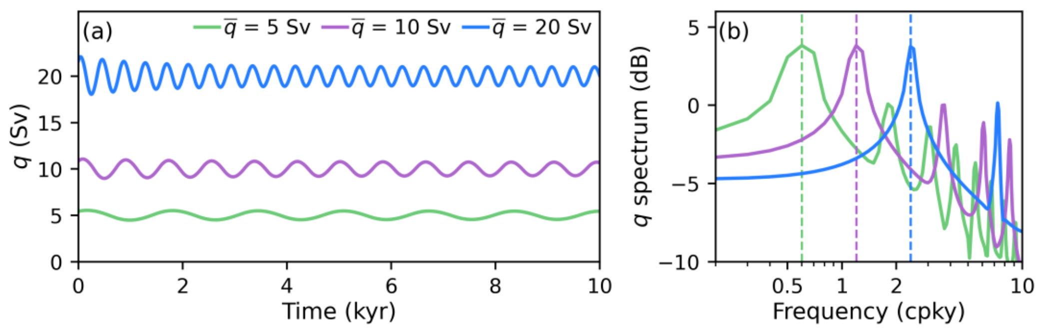

FIG. 3. (a) Time series of the q for $\bar{q}$ = 5, 10 and 20 Sv. "kyr" denotes thousand years. (b) Power spectrum of q corresponding to the simulations shown in (a), "cpky" denotes cycle per thousand years. The vertical dashed green, purple, and blue lines indicate the peak frequencies of the corresponding spectra.

The physical evolution of the oscillation remains essentially the same as that described by Li and Yang (2022), Yang et al. (2024), and Zhou et al. (2026), and is therefore not repeated here. Weakening the mean AMOC primarily lengthens the intrinsic adjustment timescale without altering the underlying feedback mechanism. Consequently, the multicentennial eigenmode identified under the reference climate state evolves naturally into a self-sustained millennial oscillation under a sufficiently weak AMOC background.

The pathway described above relies on a substantially weakened mean AMOC and a weakly unstable oscillatory mode. We next examine a fundamentally different pathway, in which an intrinsically millennial eigenmode is strongly damped under the reference climate state but becomes weakly damped through feedback from the AABW cell.

4. Weakly damped millennial oscillations induced by AABW feedback

To isolate the influence of the AABW cell, we now consider the complementary limiting case in which variability associated with the NADW cell is negligible, and the AMOC anomaly arises primarily from changes in the AABW cell,

$$q' \approx q'_{AABW} \quad \text{and} \quad q'_{NADW} \approx 0. \tag{8}$$

Under this assumption, the overturning anomaly is determined primarily by the response of the AABW cell to changes in the large-scale meridional density gradient and is parameterized as,

$$q'_{AABW} = \mu \Delta\rho', \quad \mu < 0 \tag{9}$$

Here, μ is a linear closure parameter that quantifies the sensitivity of the AABW-induced AMOC anomaly to changes in the meridional density gradient. This parameter is negative because the AABW cell opposes the NADW cell in the global overturning circulation. Unlike the NADW pathway examined in Section 3, the objective here is not to modify the mean oscillation timescale directly, but to investigate how the AABW feedback alters the stability of the intrinsic millennial eigenmode.

Previous studies have suggested that the NADW and AABW cells tend to vary out of phase: a stronger NADW cell is often accompanied by a weaker AABW cell, and vice versa (Brix and Gerdes 2003; Fieg and Gerdes 2001; Rahmstorf 2002). This anticorrelation reflects the well-known dynamical compensation between the upper and lower branches of the global overturning circulation. If the NADW-induced AMOC anomaly can be parameterized by the large-scale meridional density gradient, it is reasonable to assume that the AABW-induced anomaly can be also determined by the same density contrast but with the opposite sign. The physical basis of this parameterization is further supported by coupled climate model (CESM1.0) results presented in Appendix B.

The present treatment is conceptually analogous to classical abyssal circulation theories, such as the Stommel–Arons framework (Stommel and Arons 1959), in which the deep circulation is considered independently while the upper ocean is treated as relatively passive. A similar conceptual simplification is adopted in the reversed 1.5-layer reduced-gravity model for wind-driven circulation, where the upper layer is assumed to be nearly motionless and the lower layer carries the dynamical adjustment. Likewise, the AABW cell is not explicitly resolved in the present six-box model; instead, its influence on the AMOC is represented through the simple linear parameterization in Eq. (9).

a. Effects of Southern Ocean freshening on the intrinsic eigenmode

To examine how AABW feedback modifies the intrinsic millennial eigenmode, we perform a series of linear stability analyses under a strong-overturning background ($\bar{q} = 20\ Sv$) and a slightly saltier North Atlantic ($\bar{S_1} = 34.9\ psu$). Three background salinity states are considered by prescribing the mean salinity of the upper South Atlantic box ($\bar{S_3}$) as 33.8, 30.8, and 27.8 psu. The latter two cases represent idealized Southern Ocean freshening associated with enhanced Antarctic meltwater input.

Before considering AABW feedback, we first examine the limiting case $\mu = 0$, in which the AABW cell is completely decoupled from AMOC variability. In this limit, the least damped oscillatory mode has a period of approximately 630 years (ω_i = 3.2×10^{-10} s^{-1}) in all three experiments (Fig. 4b), demonstrating that the multicentennial eigenmode already exists as an intrinsic mode of the AMOC system. Therefore, any subsequent changes produced by nonzero μ reflect modifications of this intrinsic mode rather than the generation of a new oscillation.

As μ becomes increasingly negative, corresponding to an increased sensitivity of the AABW cell to density anomalies, the period of this mode progressively increases. In the control case ($\bar{S_3}$ = 33.8 psu), the period reaches approximately 1360 years when μ = –20 Sv kg^{-1} m^3 (ω_i = 1.5×10^{-10} s^{-1}; red curve in Fig. 4b). Thus, the intrinsic multicentennial AMOC mode is shifted to a millennial timescale by the AABW feedback.

The millennial mode in the control case is strongly damped with an e-folding decay scale of only about 110 years (ω_r = –3.0×10^{-10} s^{-1}, Fig. 4a, red curve). However, as the Southern Ocean becomes progressively fresher (i.e., with decreasing $\bar{S_3}$), the AABW feedback exerts a stronger influence on the intrinsic AMOC oscillatory mode and substantially reduces its damping rate. For example, when $\bar{S_3}$ = 30.8 psu (Fig. 4a, green curve), the e-folding damping timescale of the millennial mode increases to about 260 years (ω_r = –1.2×10^{-10} s^{-1}) at μ = –20 Sv kg^{-1} m^3. Under a sufficiently freshened Southern Ocean background ($\bar{S_3}$ = 27.8 psu, Fig. 4a, purple curve), weakly damped millennial modes appear. At μ = –12 Sv kg^{-1} m^3, the least damped mode has a period of about 1000 years (ω_i = 1.9×10^{-10} s^{-1}) and an e-folding damping timescale of about 1400 years (ω_r = –0.2×10^{-10}

s^{-1}). For sufficiently negative values of μ, however, the oscillatory mode disappears and is replaced by purely growing or decaying modes, indicating a bifurcation of the system (Fig. 4a).

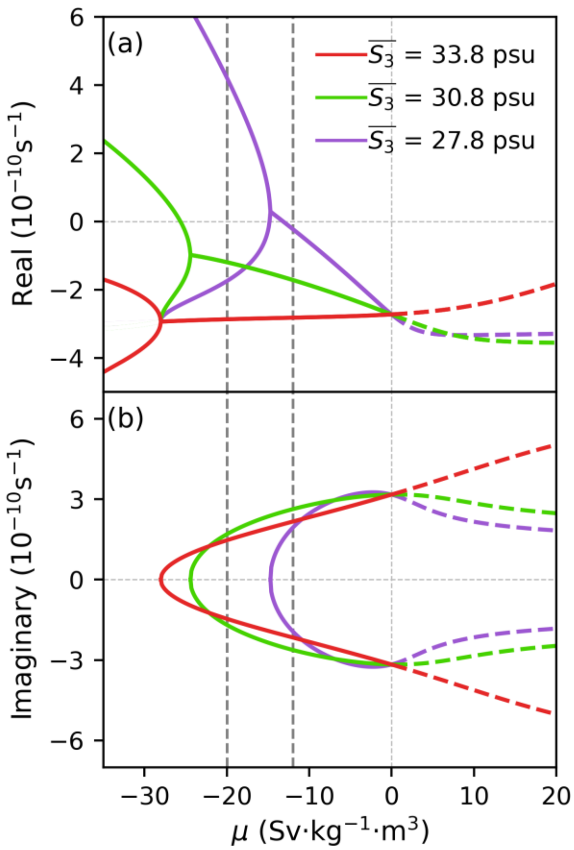

FIG. 4. Dependence of (a) the real parts and (b) the imaginary parts of the conjugate eigenvalues on μ (units: Sv kg^{-1} m^3) for the least damped oscillatory modes in the two-hemispheric model using the parameters in Table 1. The vertical dashed lines correspond to λ = –20, –12 Sv kg^{-1} m^3. The units of the ordinate are 10^{-10} s^{-1}.

The dynamical consequences of these different damping rates are illustrated in Fig. 5 for two representative cases with μ = –12 Sv kg^{-1} m^3. The mean salinity of the upper South Atlantic box is prescribed as $\overline{S_3}$ = 33.8 psu (Fig. 5a–c) and $\overline{S_3}$ =27.8 psu (Fig. 5d–f), respectively. For $\overline{S_3}$ = 33.8 psu, the least damped oscillatory mode has a period of about 920 years but an e-folding damping timescale of only about 110 years ($\omega \approx (-2.8 \pm i2.2) \times 10^{-10}$). Consequently, the oscillation decays rapidly and becomes negligible within a few hundred years, well before completing a full oscillation cycle. In contrast, for $\overline{S_3}$ =27.8 psu, the least damped mode has a comparable period of about 1030 years but a much longer damping timescale of about 1400 years ($\omega \approx (-0.2 \pm i1.9) \times 10^{-10}$).

In summary, under a strongly freshened Southern Ocean background, the damping timescale can exceed the oscillation period, allowing millennial-scale variability to persist over multiple cycles. This result demonstrates that the climatic significance of a millennial mode depends not only on its period, but also on its damping rate. The AABW feedback therefore does not generate a distinct oscillatory mode; instead, it modifies the intrinsic AMOC eigenmode by lengthening its period and, more importantly, substantially reducing its damping. Under sufficiently strong Southern Ocean freshening, such variability may become dynamically significant, leave detectable signatures in paleoclimate records, and provide a plausible dynamical mechanism for Bond-cycle variability during warm climate periods.

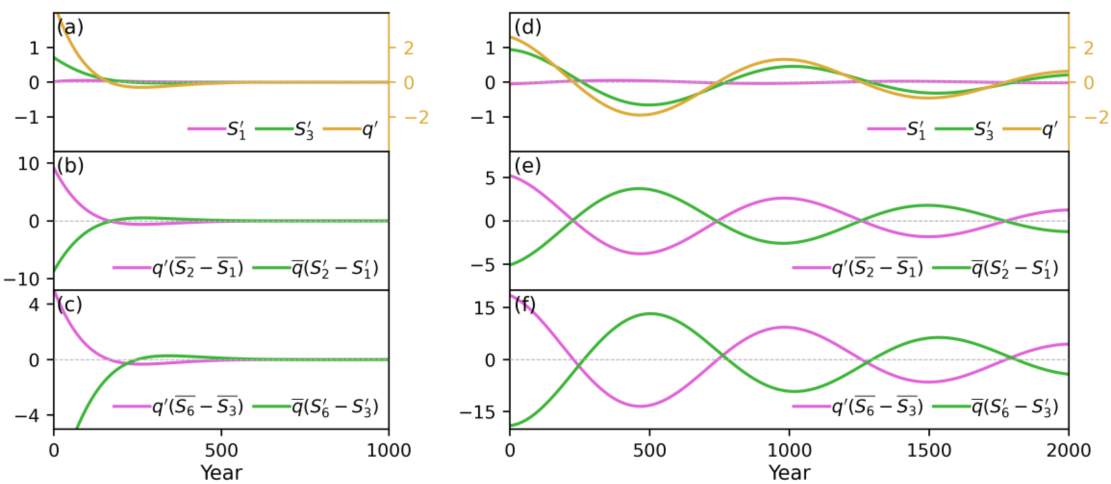

FIG. 5. Damped oscillations following an initial perturbation in the 6-box model for $\overline{S_3}$ = 33.8 psu (a-c) and $\overline{S_3}$ = 27.8 psu (d-f). (a, d) Oscillations of S_1', S_3' and q'. (b, e) Oscillations of salinity terms (units: Sv psu) in the subpolar North Atlantic: $q'(\overline{S_2}-\overline{S_1})$ and $\overline{q}(S_2'-S_1')$, which are on the right-hand side of Eq. (1a). (c, f) Oscillations of salinity terms (units: Sv psu) in the subpolar South Atlantic: $q'(\overline{S_6}-\overline{S_3})$ and $\overline{q}(S_6'-S_3')$, which are on the right-hand side of Eq. (1c).

b. Physical mechanism for damping reduction

The physical origin of the reduced damping under a freshened Southern Ocean background ($\overline{S_3}$ =27.8 psu) is illustrated in Fig. 5d–f. The salinity anomaly in the upper South Atlantic (S_3') is much larger than that in the North Atlantic (S_1') (Fig. 5d), indicating that the AABW pathway dominates the evolution of the AMOC anomaly. Consequently, the dynamical balance controlling the oscillation shifts from the North Atlantic to the Southern Ocean.

In the North Atlantic, both the perturbation-advection term and the mean-advection term act as negative feedbacks (Fig. 5e). Consider an initial positive anomaly in q'. The positive q' leads to a positive perturbation advection $[q'(\overline{S_2} - \overline{S_1})]$, enhancing S_1'. The resulting positive salinity anomaly subsequently weakens q', thereby closing the negative-feedback loop. The mean advection $[\overline{q}(S_2' - S_1')]$ also plays as a negative feedback because the induced salinity tendency opposes the existing S_1' anomaly.

In contrast, the perturbation-advection term in the South Atlantic constitutes the only positive feedback capable of compensating the damping of the intrinsic millennial eigenmode (Fig. 5f). A positive AMOC anomaly enhances the transport of the mean salinity contrast $[q'(\overline{S_6} - \overline{S_3})]$, producing a positive S_3', which further strengthens the AABW-induced overturning anomaly q'. This positive feedback is eventually balanced by the mean-advection term $[\overline{q}(S_6' - S_3')]$, preventing unlimited growth and maintaining an oscillatory adjustment.

Overall, Southern Ocean freshening amplifies the only positive perturbation-advection feedback associated with the AABW pathway without fundamentally changing the oscillation mechanism. Instead, it weakens the net damping of the intrinsic millennial eigenmode, allowing perturbations to persist over multiple oscillation cycles. Under the control salinity ($\overline{S_3}$ = 33.8 psu), this positive feedback is too weak to overcome the strong damping (Fig. 5c) (since $(\overline{S_6} - \overline{S_3})$ is small), and the oscillation decays rapidly. As the Southern Ocean becomes fresher (i.e., $(\overline{S_6} - \overline{S_3})$ become larger), however, the enhanced AABW feedback substantially reduces the damping rate, producing the weakly damped millennial mode identified in Fig. 4.

c. Sustained millennial oscillations forced by stochastic forcing

Unlike the weakly unstable mode discussed in Section 3, which requires nonlinear damping to limit its growth, the weakly damped millennial mode identified above cannot maintain finite-amplitude variability without a continuous energy source. In the climate system, however, the ocean is continually subjected to stochastic forcing arising from atmospheric variability, sea-ice fluctuations, and other climate processes. Such forcing can continuously supply energy to damped oceanic modes and maintain oscillations at their intrinsic timescales (e.g., Griffies and Tziperman 1995; Li and Yang 2022).

To represent this forcing, we introduce stochastic freshwater into the subpolar South Atlantic. Eq. (1c) is then rewritten as follows,

$$V_3\dot{S}_3' = \cdots + V_3 N \tag{10}$$

where N denotes the external stochastic forcing, represented here as Gaussian white noise.

The stochastic forcing transforms the damped oscillations in Fig. 5 into sustained millennial-scale variability (Fig. 6) by continuously replenishing the energy lost through damping. Importantly, the dominant oscillation period is nearly identical to that predicted by the linear stability analysis, demonstrating that the stochastic forcing excites an intrinsic eigenmode of the AMOC rather than imposing its own characteristic timescale.

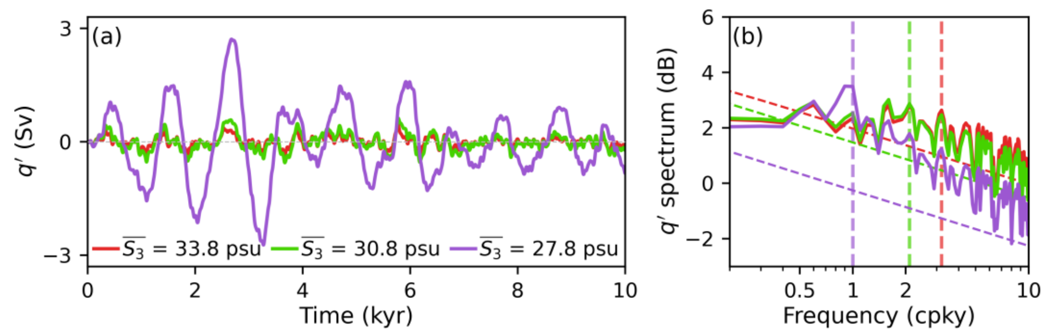

FIG. 6. Time series of (a) q' and in the two-hemispheric box model, forced by stochastic freshwater flux injected in the box 3 (South Atlantic) under different $\overline{S_3}$. μ is set to –12 Sv kg^{-1} m^{3}. Other parameters are shown in Table 1. (b) Power spectra of q' for different cases with the confidence level 95% (denoted by dashed curves). Vertical lines indicate the peak frequencies of the corresponding spectra.

The response amplitude depends strongly on the damping rate of the intrinsic millennial mode. When $\overline{S_3}$ = 33.8 psu, the eigenmode is strongly damped. Although stochastic forcing sustains a persistent oscillation, its amplitude remains small (Fig. 6a, red curve). As the Southern Ocean freshens progressively, the damping weakens, leading to a much stronger response to stochastic forcing. For $\overline{S_3}$ = 27.8 psu, the maximum AMOC anomaly reaches approximately 2 Sv (purple curve), demonstrating that weakly damped modes are much more readily excited than strongly damped ones.

These results help explain why some intrinsic oceanic modes are expressed in paleoclimate records whereas others remain undetectable. Strongly damped modes dissipate before reaching appreciable amplitudes, even under continuous stochastic forcing, whereas weakly damped modes can accumulate energy over many oscillation cycles and become dynamically significant. Here, we show that a substantially freshened Southern Ocean can provide favourable conditions for millennial-scale variability to leave detectable signatures in paleoclimate records.

An important implication is that extensive freshwater input from Antarctic sea ice or continental ice sheets may shift the climate system toward a weakly damped regime in which intrinsic millennial variability becomes readily excitable. This mechanism offers a plausible dynamical explanation for Bond-cycle variability during warm climate periods.

5. Summary and discussion

This study proposes a new dynamical framework for understanding Bond-cycle variability based on intrinsic AMOC eigenmodes. Linear stability analysis of a two-hemisphere six-box model reveals that the AMOC possesses two intrinsic oscillatory eigenmodes: a weakly unstable multicentennial mode and a strongly damped millennial mode. Rather than invoking a distinct mechanism operating only on millennial timescales, our results suggest that Bond-cycle variability may arise from modifications of these intrinsic eigenmodes under different background climate states.

The two eigenmodes reach millennial timescales through two complementary pathways. The first pathway involves the weakly unstable multicentennial mode. As the mean AMOC weakens, its intrinsic adjustment timescale increases, allowing the oscillation period to shift naturally from several hundred years to more than one thousand years. When weak nonlinear damping is included, this millennial mode evolves into a finite-amplitude self-sustained oscillation. The second pathway involves the strongly damped millennial mode. Feedback from the AABW cell does not generate a new oscillatory mode, but instead modifies the intrinsic eigenmode by lengthening its period and, more importantly, substantially reducing its damping. Under a sufficiently freshened Southern Ocean background, stochastic forcing can efficiently excite this weakly damped mode and produce persistent millennial-scale variability comparable to the Bond cycle.

One important implication of this study is that the climatic significance and observability of an intrinsic climate mode depend not only on its characteristic period, but also on its damping rate. An intrinsic millennial mode may exist over a broad range of climate states, yet strongly damped modes are unlikely to leave detectable signatures in paleoclimate records because perturbations decay before reaching appreciable amplitudes. By contrast, weakly damped modes can accumulate energy from stochastic forcing over many oscillation cycles and become dynamically significant. This perspective offers a possible explanation for the apparent discrepancy between proxy records, which contain widespread evidence of Bond-cycle variability, and coupled climate models, in which millennial-scale oscillations are often weak or absent.

Our results are broadly consistent with previous studies emphasizing the importance of Southern Ocean processes in millennial-scale climate variability. Millennial variability associated with Antarctic Circumpolar Deep Water (Khider et al. 2014), Southern Ocean convection (Drijfhout et al. 1996), and interactions between the NADW and AABW cells (Melcher et al. 2025; Vettoretti et al. 2022) all point to an active role of the Southern Hemisphere in regulating low-frequency overturning variability. Likewise, relatively small perturbations originating in the Southern Ocean have been shown to induce large AMOC responses (Dima et al. 2018; Thomas et al. 2011). Our results provide a unified dynamical interpretation of these studies by showing that Southern Ocean freshening primarily modifies the stability properties of intrinsic AMOC eigenmodes, rather than creating a fundamentally new oscillation. More generally, they suggest that millennial-scale climate variability is controlled by the evolution of the entire global overturning circulation rather than by processes confined to the North Atlantic alone.

Although highly idealized, the present framework may also have implications for future climate change. Continued Antarctic sea-ice loss and ice-sheet melting are expected to freshen the Southern Ocean and weaken AABW formation. If sufficiently large, such changes may shift the overturning circulation toward a weakly damped regime in which intrinsic millennial modes become more readily excitable. While this does not imply that Bond-cycle variability will occur under future warming, it suggests that cryospheric changes may favor the emergence of enhanced low-frequency climate variability through their influence on the stability of the overturning circulation.

Several important questions remain unresolved. First, the mechanisms identified here are derived from an idealized conceptual model and should be tested in comprehensive coupled climate models. Second, although our results highlight the dynamical role of Southern Ocean freshening, the magnitude and timing of freshwater input during past Bond events remain uncertain and require further constraints from proxy reconstructions. Third, millennial-scale climate variability is likely influenced by interactions among multiple components of the climate system, including AMOC dynamics, AABW feedback, sea ice (Ganopolski and Rahmstorf 2001; Vettoretti and Peltier 2016; Vettoretti et al. 2022), ice sheets (Petersen et al. 2013), atmospheric circulation, and external forcing (Arzel et al. 2010; Olsen et al. 2005). Understanding how these processes interact to regulate the period, damping, and excitation of intrinsic AMOC eigenmodes remains an important challenge for future research.

Overall, this study suggests that Bond-cycle variability may arise from the stochastic excitation of intrinsic AMOC eigenmodes whose characteristic timescales and damping properties are strongly controlled by the background overturning state. By distinguishing the respective roles of eigenmode generation, mean-state modulation, and stochastic excitation, this framework provides a new perspective on the origin of Holocene millennial climate variability and establishes a physically consistent link between conceptual theory, proxy evidence, and coupled climate model simulations.

Acknowledgements.

This research is jointly supported by the NSF of China (Nos. 42230403, 42288101, 41725021, and 91737204) and by the foundation at the Shanghai Frontiers Science Centre of Atmosphere-Ocean Interaction of Fudan University.

Data Availability Statement.

All data and codes used in this study are available upon request.

Conflict of interest

The authors have no relevant financial or non-financial interests to disclose.

APPENDIX A

Nonlinear vertical mixing and sustained AMOC oscillations

The linear stability analysis presented in the main text identifies the intrinsic oscillatory modes of the system, but, by itself, does not produce sustained oscillations. A linearly stable mode ultimately decays to zero, whereas a weakly unstable mode grows without bound in the absence of nonlinear processes. To obtain finite-amplitude sustained oscillations, an additional nonlinear stabilization mechanism is required.

Several approaches have been proposed for this purpose in conceptual models. In this study, we adopt the nonlinear vertical-mixing parameterization introduced by Li and Yang (2022). Their approach assumes that the effective vertical mixing in the subpolar North Atlantic increases with the magnitude of the AMOC anomaly, thereby counteracting the positive salinity-advection feedback that drives the instability. The mixing coefficient is represented by a quadratic function of the AMOC anomaly.

The quadratic formulation is supported by both numerical and physical considerations. Regression analysis of a coupled climate model indicates that the effective mixing increases approximately symmetrically for positive and negative AMOC anomalies (Li and Yang 2022). Physically, when the stratification in the subpolar ocean is weak and the AMOC is strong, upper-ocean salinity anomaly can be mixed into the deeper ocean more efficiently by salinity diffusion. When the stratification in the subpolar ocean is strong and the AMOC is weak, the salinity diffusion is weak but the eddy-induced salinity mixing can enhance the downward mixing. Although the underlying mechanisms differ, both strong and weak AMOC enhance effective mixing. A quadratic parameterization a simple and physically consistent representation of this approximately symmetric behavior. The salinity equation of the subpolar North Atlantic can be rewritten as:

$$V_1\dot{S}_1' = \bar{q}(S_2' - S_1') + q'(\bar{S}_2 - \bar{S}_1) - k_m(S_1' - S_4') \tag{A1a}$$

$$V_4\dot{S}_4' = \bar{q}(S_1' - S_4') + k_m(S_1' - S_4') \tag{A1b}$$

$$k_m = \kappa q'^2 \tag{A1c}$$

where κ is a positive constant and is set to 10^{-4} $\mathrm{m^{-3}\,s}$ in this paper to tune the desire oscillation amplitude. It can be even set to be an order of smaller, indicating that even weak subpolar vertical mixing can convert a growing oscillation into a self-sustained one. As a result, k_m is always positive and represents a process that always transfers the salinity anomaly of upper ocean downward to lower ocean, no matter whether the AMOC is stronger or weaker than usual.

For example, for $\bar{q}$ = 10 Sv and λ = 8.9 Sv kg^{-1} m^3, the time series of salinity anomalies show oscillations with periods about 1000 years and an exponentially growing amplitude (dashed grey curve in Fig. A1), as predicted by the eigenvalues discussed in section 2. After adding the enhanced mixing in the subpolar North Atlantic, the unstable oscillation becomes a self-sustained oscillation with a limited amplitude (solid curve in Fig. A1).

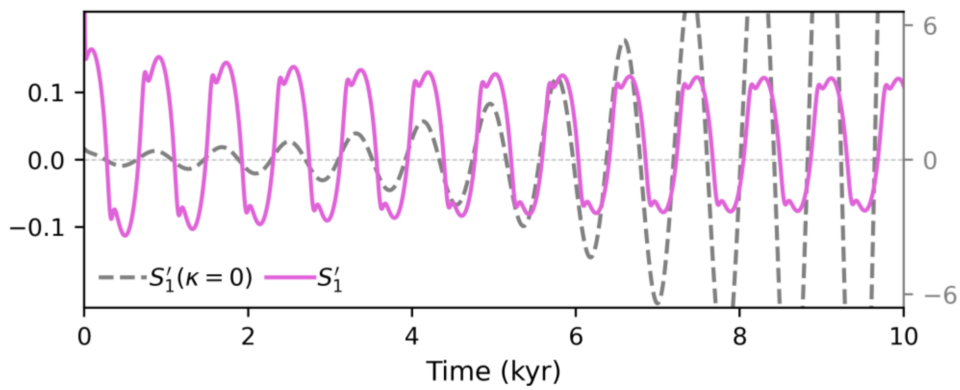

FIG. A1. Unstable oscillation of S_1' (dashed curve; units: psu) in the two-hemispheric model without enhanced vertical mixing ($\kappa = 0$) in the subpolar North Atlantic; self-sustained oscillations of S_1' (solid curve) with the enhanced vertical mixing.

APPENDIX B

Coupled model evaluation of the NADW–AABW parameterization

Eq. (5) assumes that AMOC variability consists of NADW- and AABW-related components, both linked to the large-scale meridional density gradient. While this parameterization is physically motivated, its applicability to a comprehensive coupled climate model has not yet been examined. Here, we evaluate the proposed parameterization using a long preindustrial control simulation of the Community Earth System Model (CESM, version 1.0).

The CESM simulation is integrated for 2500 years under preindustrial boundary conditions. Following model spin-up, the last 1900 years are analyzed to investigate internally generated low-frequency variability. The ocean component has a nominal horizontal resolution of approximately 1°, with a zonal spacing of 1.125° and a meridional spacing varying from 0.27° near the equator to about 0.65° at 60°N/S before gradually decreasing toward the poles. A detailed description of the model configuration is given by Yang et al. (2015).

The time series of the AMOC, AABW, and Atlantic salinity were extracted and then low-pass filtered with a 30-year cutoff. The coupled-model results are then used to examine the relationships among these quantities and to assess the physical basis of the parameterization adopted in the conceptual model.

Assuming that the low-frequency salinity anomaly in the Atlantic is controlled by overturning-induced salt transport, the salinity tendency can be written as:

$$\frac{dS'}{dt} = \alpha_N q_N' + \alpha_A q_A' - \frac{S'}{\tau_s} + \varepsilon \tag{B1}$$

where S' denotes the low-pass-filtered Atlantic salinity anomaly (can be integrated over any depth), q_N' and q_A' denote the anomalies of NADW and AABW cells, respectively, τ_s is the effective restoring timescale associated with mixing and diffusion, and ε represents unresolved processes.

Eq. (B1) assumes that low-frequency salinity changes arise primarily from the combined effects of the NADW and AABW overturning cells, while all remaining processes are represented by a linear restoring term and a residual. The coefficients α_N, α_A and τ_s are estimated by multiple linear regression. For simplicity, no time lag is introduced because the low-pass filtering largely removes high-frequency adjustment processes.

Once these coefficients are determined, the salinity anomalies associated with the NADW and AABW cells are reconstructed separately from:

$$\frac{dS'_N}{dt} = \alpha_N q'_N - \frac{S'_N}{\tau_s} \tag{B2a}$$

$$\frac{dS'_A}{dt} = \alpha_A q'_A - \frac{S'_A}{\tau_s} \tag{B2b}$$

respectively, with zero initial conditions. The reconstructed components satisfy approximately

$$S' \approx S'_N + S'_A + S'_{res} \tag{B3}$$

where S'_{res} denotes the residual component associated with unresolved processes. This decomposition enables us to quantify separately the contributions of the NADW and AABW cells to the low-frequency salinity variability simulated by the coupled climate model.

The corresponding time discretized forms of (B2) are

$$S'_N(t + \Delta t) = S'_N(t) + \Delta t \left[\alpha_N q'_N(t) - \frac{S'_N}{\tau_s}\right] \tag{B4a}$$

$$S'_A(t + \Delta t) = S'_A(t) + \Delta t \left[\alpha_A q'_A(t) - \frac{S'_A}{\tau_s}\right] \tag{B4b}$$

with initial condition:

$$S'_N(t = 0) = 0, \quad S'_A(t = 0) = 0$$

In the calculation, q'_N is defined as anomaly of the maximum overturning streamfunction within 20 to 70°N and 300 to 2000 m depth. q'_A is defined as anomaly of the magnitude of the minimum of the global meridional overturning streamfunction south of 34.5°S and deeper than 1000 m. S' is vertically-weighted averaged over the entire ocean depth.τ_s is given as 30 years. Δt is set to 1 year.

Figure B1 shows the regression coefficients α_N and α_A obtained from Eq. (B1), which quantify the sensitivities of the upper Atlantic salinity tendency to variations in the NADW and AABW cells, respectively. The largest coefficients are concentrated in the NADW formation region (green rectangle). There, α_N is predominantly positive, indicating that a stronger NADW cell increases the upper-ocean salinity through enhanced northward salt transport. In contrast, α_A exhibits nearly opposite signs over the same region, implying that a stronger AABW cell acts to reduce the upper-ocean salinity. The approximately mirror-image regression patterns demonstrate that the NADW and AABW cells exert competing influences on the upper Atlantic salinity, providing direct support for the opposite-sign parameterization adopted in the conceptual model.

In the Southern Ocean (yellow rectangle), α_N is close to zero, whereas α_A exhibits a coherent signal. This contrast reflects the distinct dynamical influences of the two overturning cells: AABW primarily modulates salinity in the Southern Ocean, while the strongest NADW influence is concentrated in the NADW formation region.

Together, these regression patterns indicate that the NADW and AABW cells influence upper Atlantic salinity in physically distinct yet dynamically complementary ways. Their opposing effects in the NADW formation region provide supports for the NADW–AABW parameterization adopted in the conceptual model.

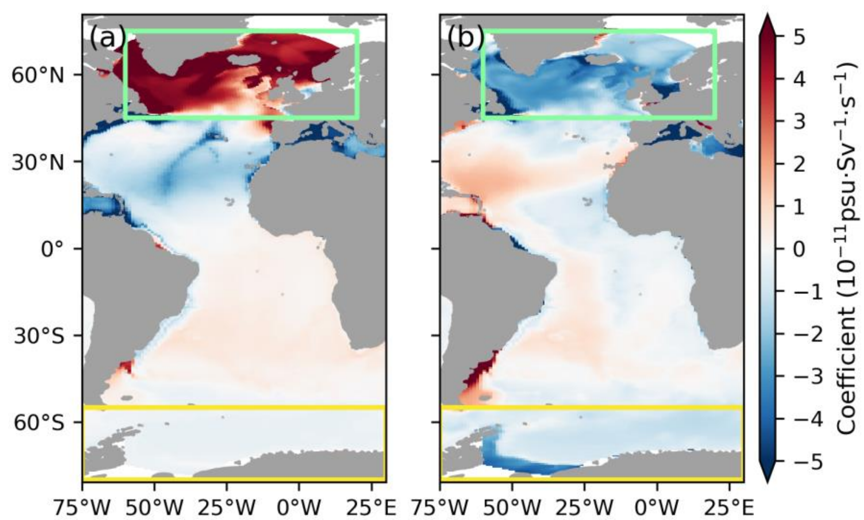

FIG. B1. Regression coefficients of the (a) α_N and (b) α_A (units: 10^{-11} psu Sv^{-1} s^{-1}).

Figure B2 compares the NADW and AABW anomalies with the meridional salinity differences between the subpolar North Atlantic (green rectangle in Fig. B1) and the subpolar South Atlantic (yellow rectangle). The salinity differences between the North Atlantic box (green) and South

Atlantic box (yellow) associated with the NADW and AABW cells, denoted by $\Delta S_N'$ and $\Delta S_A'$, are reconstructed from Eq. (B4).

As shown in Figs. B2a and B2b, both q_N' and q_A' exhibit linear relationships with $\Delta S_N'$+$\Delta S_A'$, yielding regression coefficients of 39.8 and −9.8 Sv kg^{-1} m^3, respectively. These coefficients correspond directly to the closure parameters λ and μ in Eqs. (2) and (9), providing quantitative support for the parameterization adopted in the conceptual model. Here, we would like to emphasize that $\Delta\rho'$ (or $\Delta S'$) in the conceptual model corresponds to $(\Delta S_N' + \Delta S_A')$ in the coupled model.

The reconstructed overturning anomalies, $\lambda(\Delta S_N'$+$\Delta S_A')$ and $\mu(\Delta S_N'$+$\Delta S_A')$, closely reproduce the model output q_N' and q_A' (Fig. B2c). In addition, q_N' and q_A' are negatively correlated, consistent with the well-established dynamical compensation between the upper and lower branches of the global overturning circulation. A slight phase lag exists between the model output and reconstructed anomalies, which is expected because the linear parameterization neglects the finite adjustment time between overturning-induced salt transport and the subsequent density response. It also reflects the finite salinity adjustment timescale represented by τ_S. Overall, these results demonstrate that the large-scale meridional salinity gradient is a useful predictor for both NADW and AABW variability and supports the physical basis of the NADW–AABW parameterization used in the conceptual model. Here, we would like to emphasize that, although the AABW variability is considerably weaker than the NADW variability, its dependence on the large-scale salinity gradient remains well described by the linear parameterization.

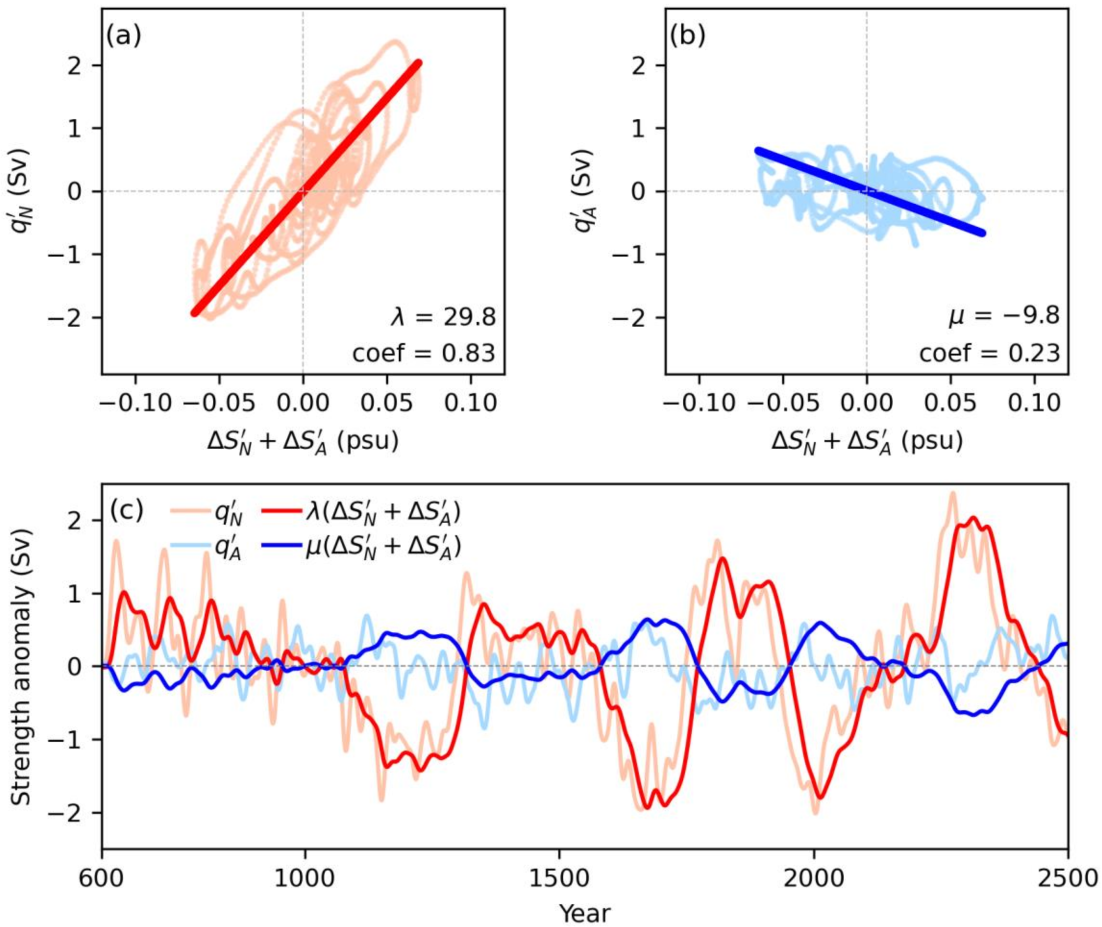

FIG. B2. Scatter plots of (a) q'_N and (b) q'_A versus the salinity difference $\Delta S'_N$+$\Delta S'_A$ between the subpolar North and South Atlantic oceans. The red (blue) line denotes the linear regression with a slope of 29.8 (–9.8) Sv psu^{-1}. (c) Time series of original q'_N (light red) and q'_A (light blue) from model output, together with their estimations derived from the linear regressions (red and blue). q'_N and q'_A and $\Delta S'_N$+$\Delta S'_A$ were low-pass filtered using a 30-year cutoff period.

REFERENCES

Arzel, O., A. Colin De Verdière, and M. H. England, 2010: The Role of Oceanic Heat Transport and Wind Stress Forcing in Abrupt Millennial-Scale Climate Transitions. *J. Climate*, **23,** 2233-2256, 10.1175/2009jcli3227.1.

Bond, G., and Coauthors, 1997: A pervasive millennial-scale cycle in North Atlantic Holocene and glacial climates. *Science*, **278,** 1257-1266, 10.1126/science.278.5341.1257.

Brix, H., and R. Gerdes, 2003: North Atlantic Deep Water and Antarctic Bottom Water: Their interaction and influence on the variability of the global ocean circulation. *J. Geophys. Res.: Oceans*, **108,** n/a-n/a, 10.1029/2002jc001335.

Colin de Verdière, A., 2007: A simple model of millennial oscillations of the thermohaline circulation. *J. Phys. Oceanogr.*, **37,** 1142-1155

Colin De Verdière, A., and L. Te Raa, 2010: Weak oceanic heat transport as a cause of the instability of glacial climates. *Climate Dyn.*, **35,** 1237-1256, 10.1007/s00382-009-0675-8.

Dansgaard, W., S. Johnsen, H. Clausen, D. Dahl-Jensen, N. Gundestrup, C. Hammer, and H. Oeschger, 1984: North Atlantic climatic oscillations revealed by deep Greenland ice cores. *Climate processes and climate sensitivity*, J. Hansen, and T. Takahashi, Eds., 288-298.

Debret, M., and Coauthors, 2007: The origin of the 1500-year climate cycles in Holocene North-Atlantic records. *Clim. Past*, **3,** 569-575, 10.5194/cp-3-569-2007.

Dima, M., G. Lohmann, and G. Knorr, 2018: North Atlantic Versus Global Control on Dansgaard-Oeschger Events. *Geophys. Res. Lett.*, **45,** 12,991–912,998, 10.1029/2018gl080035.

Drijfhout, S., C. Heinze, M. Latif, and E. Maier-Reimer, 1996: Mean Circulation and Internal Variability in an Ocean Primitive Equation Model. *J. Phys. Oceanogr.*, **26,** 559-580, 10.1175/1520-0485(1996)026<0559:mcaivi>2.0.co;2.

Fieg, K., and R. Gerdes, 2001: Sensitivity of the thermohaline circulation to modern and glacial surface boundary conditions. *J. Geophys. Res.: Oceans*, **106,** 6853-6867, 10.1029/1999jc000102.

Frajka-Williams, E., S. A. Cunningham, H. Bryden, and B. A. King, 2011: Variability of Antarctic Bottom Water at 24.5°N in the Atlantic. *J. Geophys. Res.: Oceans*, **116**, 10.1029/2011jc007168.

Friedrich, T., A. Timmermann, L. Menviel, O. Elison Timm, A. Mouchet, and D. M. Roche, 2010: The mechanism behind internally generated centennial-to-millennial scale climate variability in an earth system model of intermediate complexity. *Geoscientific Model Development*, **3,** 377-389, 10.5194/gmd-3-377-2010.

Ganopolski, A., and S. Rahmstorf, 2001: Rapid changes of glacial climate simulated in a coupled climate model. *Nature*, **409,** 153-158, 10.1038/35051500.

——, 2002: Abrupt glacial climate changes due to stochastic resonance. *Phys. Rev. Lett.*, **88,** 038501, 10.1103/PhysRevLett.88.038501.

Gottwald, G. A., 2021: A model for Dansgaard–Oeschger events and millennial-scale abrupt climate change without external forcing. *Climate Dyn.*, **56,** 227-243, 10.1007/s00382-020-05476-z.

Griffies, S. M., and E. Tziperman, 1995: A linear thermohaline oscillator driven by stochastic atmospheric forcing. *J. Climate*, **8,** 2440-2453, 10.1175/1520-0442(1995)008<2440:ALTODB>2.0.CO;2.

Huang, R. X., J. R. Luyten, and H. M. Stommel, 1992: Multiple equilibrium states in combined thermal and saline circulation. *J. Phys. Oceanogr.*, **22,** 231-246, 10.1175/1520-0485(1992)022<0231:MESICT>2.0.CO;2.

Khider, D., C. S. Jackson, and L. D. Stott, 2014: Assessing millennial-scale variability during the Holocene: A perspective from the western tropical Pacific. *Paleoceanography*, **29,** 143-159, 10.1002/2013pa002534.

Klockmann, M., U. Mikolajewicz, H. Kleppin, and J. Marotzke, 2020: Coupling of the Subpolar Gyre and the Overturning Circulation During Abrupt Glacial Climate Transitions. *Geophys. Res. Lett.*, **47,** e2020GL090361, 10.1029/2020gl090361.

Li, Y., and H. Yang, 2022: A Theory for Self-Sustained Multicentennial Oscillation of the Atlantic Meridional Overturning Circulation. *J. Climate*, **35,** 5883-5896, 10.1175/jcli-d-21-0685.1.

Lucarini, V., and P. H. Stone, 2005a: Thermohaline circulation stability: a box model study. Part II: coupled atmosphere–ocean model. *J. Climate*, **18,** 514-529, 10.1175/JCLI-3279.1.

——, 2005b: Thermohaline circulation stability: A box model study. Part I: Uncoupled model. *J. Climate*, **18,** 501-513, 10.1175/JCLI-3278.1.

Lynch-Stieglitz, J., 2017: The Atlantic meridional overturning circulation and abrupt climate change. *Annu. Rev. Mar.*

Science, **9,** 83-104, 10.1146/annurev-marine-010816-060415.

Melcher, J. O., S. Halkjær, P. Ditlevsen, P. L. Langen, G. Vettoretti, and S. O. Rasmussen, 2025: A novel conceptual model for Dansgaard–Oeschger event dynamics based on ice-core data. *Clim. Past*, **21,** 115-132, 10.5194/cp-21-115-2025.

Olsen, S. M., G. Shaffer, and C. J. Bjerrum, 2005: Ocean oxygen isotope constraints on mechanisms for millennial-scale climate variability. *Paleoceanography*, **20,** PA1014, 10.1029/2004pa001063.

Peltier, W. R., and G. Vettoretti, 2014: Dansgaard-Oeschger oscillations predicted in a comprehensive model of glacial climate: A "kicked" salt oscillator in the Atlantic. *Geophys. Res. Lett.*, **41,** 7306-7313, 10.1002/2014gl061413.

Petersen, S. V., D. P. Schrag, and P. U. Clark, 2013: A new mechanism for Dansgaard-Oeschger cycles. *Paleoceanography*, **28,** 24-30, 10.1029/2012pa002364.

Rahmstorf, S., 2002: Ocean circulation and climate during the past 120,000 years. *Nature*, **419,** 207-214, 10.1038/nature01090.

Rivin, I., and E. Tziperman, 1997: Linear versus Self-Sustained Interdecadal Thermohaline Variability in a Coupled Box Model. *J. Phys. Oceanogr.*, **27,** 1216-1232, 10.1175/1520-0485(1997)027<1216:Lvssit>2.0.Co;2.

Sakai, K., and W. R. Peltier, 1995: A simple model of the Atlantic thermohaline circulation: Internal and forced variability with paleoclimatological implications. *J. Geophys. Res.*, **100,** 13455, 10.1029/95jc00616.

Sakai, K., and W. R. Peltier, 1996: A multibasin reduced model of the global thermohaline circulation: Paleoceanographic analyses of the origins of ice-age climate variability. *J. Geophys. Res.: Oceans*, **101,** 22535-22562, 10.1029/96JC00539.

Schulz, M., M. Prange, and A. Klocker, 2007: Low-frequency oscillations of the Atlantic Ocean meridional overturning circulation in a coupled climate model. *Clim. Past*, **3,** 97-107, 10.5194/cp-3-97-2007.

Scott, J. R., J. Marotzke, and P. H. Stone, 1999: Interhemispheric thermohaline circulation in a coupled box model. *J. Phys. Oceanogr.*, **29,** 351-365, 10.1175/1520-0485(1999)029<0351:ITCIAC>2.0.CO;2.

Sévellec, F., and A. V. Fedorov, 2014: Millennial Variability in an Idealized Ocean Model: Predicting the AMOC Regime Shifts. *J. Climate*, **27,** 3551-3564, 10.1175/jcli-d-13-00450.1.

Sévellec, F., T. Huck, and M. Ben Jelloul, 2006: On the mechanism of centennial thermohaline oscillations. *Journal of Marine Research*, **64,** 355-392, 10.1357/002224006778189608.

Stommel, H., 1961: Thermohaline convection with two stable regimes of flow. *Tellus*, **13,** 224-230, 10.1111/j.2153-3490.1961.tb00079.x.

Stommel, H., and A. Arons, 1959: On the abyssal circulation of the world ocean—I. Stationary planetary flow patterns on a sphere. *Deep Sea Research (1953)*, **6,** 140-154, 10.1016/0146-6313(59)90065-6.

Stössel, A., and S. J. Kim, 2001: Decadal deep-water variability in the subtropical Atlantic and convection in the Weddell Sea. *J. Geophys. Res.: Oceans*, **106,** 22425-22440, 10.1029/2000jc000335.

Thomas, A. M., S. Rupper, and W. F. Christensen, 2011: Characterizing the statistical properties and interhemispheric distribution of Dansgaard-Oeschger events. *J. Geophys. Res.*, **116,** D03103, 10.1029/2010jd014834.

Timmermann, A., H. Gildor, M. Schulz, and E. Tziperman, 2003: Coherent Resonant Millennial-Scale Climate Oscillations Triggered by Massive Meltwater Pulses. *J. Climate*, **16,** 2569-2585, 10.1175/1520-0442(2003)016<2569:crmcot>2.0.co;2.

Vettoretti, G., and W. R. Peltier, 2016: Thermohaline instability and the formation of glacial North Atlantic super polynyas at the onset of Dansgaard-Oeschger warming events. *Geophys. Res. Lett.*, **43,** 5336-5344, 10.1002/2016gl068891.

——, 2018: Fast Physics and Slow Physics in the Nonlinear Dansgaard–Oeschger Relaxation Oscillation. *J. Climate*, **31,** 3423-3449, 10.1175/jcli-d-17-0559.1.

Vettoretti, G., P. Ditlevsen, M. Jochum, and S. O. Rasmussen, 2022: Atmospheric CO2 control of spontaneous millennial-scale ice age climate oscillations. *Nat. Geosci.*, **15,** 300-306, 10.1038/s41561-022-00920-7.

von der Heydt, A. S., P. Ashwin, C. D. Camp, M. Crucifix, H. A. Dijkstra, P. Ditlevsen, and T. M. Lenton, 2021: Quantification and interpretation of the climate variability record. *Global Planet. Change*, **197**, 10.1016/j.gloplacha.2020.103399.

Wang, S., H. Yang, and X. Zhou, 2025: Investigating the multicentennial oscillation of the AMOC using a simplified two-dimensional ocean model. *Climate Dyn.*, **63**, 10.1007/s00382-025-07891-6.

Wang, Z., and L. A. Mysak, 2006: Glacial abrupt climate changes and Dansgaard-Oeschger oscillations in a coupled climate model. *Paleoceanography*, **21,** PA2001, 10.1029/2005pa001238.

Winton, M., and E. S. Sarachik, 1993: Thermohaline oscillations induced by strong steady salinity forcing of ocean general circulation models. *J. Phys. Oceanogr.*, **23,** 1389-1410, 10.1175/1520-0485(1993)023<1389:TOIBSS>2.0.CO;2.

Yang, H., Q. Li, K. Wang, Y. Sun, and D. Sun, 2015: Decomposing the meridional heat transport in the climate system. *Climate Dyn.*, **44,** 2751-2768, 10.1007/s00382-014-2380-5.

Yang, K., H. Yang, and Y. Li, 2024: A Theory for Self-Sustained Multicentennial Oscillation of the Atlantic Meridional Overturning Circulation. Part II: Role of Temperature. *J. Climate*, **37,** 913-926, 10.1175/jcli-d-22-0755.1.

Zhang, X., G. Lohmann, G. Knorr, and C. Purcell, 2014: Abrupt glacial climate shifts controlled by ice sheet changes. *Nature*, **512,** 290-294, 10.1038/nature13592.

Zhang, X., G. Knorr, G. Lohmann, and S. Barker, 2017: Abrupt North Atlantic circulation changes in response to gradual CO2 forcing in a glacial climate state. *Nat. Geosci.*, **10,** 518-523, 10.1038/ngeo2974.

Zhou, X., K. Yang, H. Yang, and Q. Zhang, 2026: Self-sustained multicentennial oscillation of the Atlantic meridional overturning circulation in two-hemisphere box models. *Climate Dyn.*, **64**, 10.1007/s00382-025-07947-7.